Seismic Shot Recovery via Low-Rank Tensor Modeling on the Cross-Spread Domain

Iván Ortiz[1], Tatiana Gelvez-Barrera[2], Laura Galvis[1], and Henry Arguello[1]
[1]Department of Computer Science, Universidad Industrial de Santander, Bucaramanga, Colombia.
[2] Université de Lyon, INSA-Lyon, Université Claude Bernard Lyon 1, UJM-Saint Etienne, CNRS, Inserm, CREATIS UMR 5220, U1294, F-69621, LVA, Villeurbanne, France

***Abstract*—A seismic survey captures a wave field for detecting earth properties that support geological explorations. The seismic data is acquired through the use of sources and receivers located in the study field. The captured data, organized in a 3D datacube, can be incomplete because of environmental limitations, hardware malfunction, or undetonated sources to reduce costs and environmental impact. The missing data from removed sources, so-called missing shots, has been computationally recovered by compressive-based methods that usually vectorize the datacube, destroying the natural structure and redundancies in the seismic data. This work introduces a shot recovery method for a commonly used orthogonal seismic acquisition geometry, inducing a non-local self-similarity prior through the Plug-and-Play framework (PnP). The proposed method relies on the flexibility and versatility of the PnP to employ a denoiser as the promoter of the high-structural redundancies over the 3D datacube. Experiments over a synthetic-realistic dataset show the proposed method's effectiveness, obtaining improved recovery quality and reduced computational time compared to the state-of-the-art methods.**

***Index Terms*—Plug-and-Play framework, Seismic shot recovery, Orthogonal acquisition geometry, Cross-spread domain.**

I. Introduction

Seismic surveys are used in geophysics exploration to determine the structure of subsurface rocks and soils, supporting the decision-making on oil, gas, and mineral exploration and extraction [1]. A seismic survey is acquired through the generation of seismic waves in the ground using devices called sources, then, the wave reflections and refractions are recorded by sensors called receivers.

The 3D orthogonal geometry is a seismic acquisition configuration where lines of receivers and sources are deployed in a grid pattern, with the lines crossing each other at right angles; the intersection between a line of receivers and a line of sources forms a cross-spread, a basic 3D seismic unit. The collected data can be processed to form a geophysical image [2] or organized in a 3D datacube to be computationally treated in denoising, super-resolution, and processing tasks.

Seismic surveys face several challenges, such as equipment failure, poor data quality, and gaps in the acquisition geometry by missing devices, causing the loss of information during the acquisition and consequently reducing the quality and accuracy during the posterior geophysical image generation [3].

The nature of the loss of information is an essential issue for companies conducting seismic surveys. In particular, missing receivers lead to missing seismic traces, corresponding to 1D columns in the seismic datacube, usually completed with interpolation techniques [4]. Meanwhile, undetonated sources, an exciting scenario from an economic and ecological point of view, lead to missing 2D slices, referred to as shots, in the cross-spread 3D datacube, whose reconstruction is a challenging research and industry problem yet to be explored [5].

Data processing and interpolation techniques have recently addressed the seismic shot reconstruction problem, using prior information such as sparsity on a transformation basis [6] and interpolation neural networks [7]. However, the works mentioned above usually fail in the reconstruction of the 3D structure of the cross-spread and disregard the high non-local intrinsic redundancies, a prior used to improve the accuracy of seismic noise attenuation [8] and, to a lesser extent, for seismic interpolation [4]. A possible solution is the use of a non-local self-similarity (NSS) prior, which relies on the assumption that regions with similar patterns are not necessarily located in the same spatial region [9], [10]. In a seismic array, the NSS can be attributed to the distribution of the wave phenomena across adjacent subsurface surfaces.

Therefore, this work introduces a seismic shot reconstruction algorithm that takes advantage of the NSS presented in the seismic slices of the cross-spread using a patch-based plug-and-play (PnP) framework (Section II). The PnP is introduced flexibly through a tensor factorization that enables applying the NSS prior independently through the different datacube dimensions. Experiments using a synthetic-realistic database show a better performance of the proposed algorithm, in terms of reconstruction quality and computation time-saving, compared to the state-of-the-art interpolation algorithms (Section III).

II. Plug-and-play Low-rank Prior Methodology for Seismic Shot Recovery

This section describes the mathematical modeling of the seismic acquisition process with sub-sampled shots, the formulation of the proposed optimization problem for seismic shot reconstruction, and the developed numerical algorithm. Throughout the section, definitions will use the tensor notation and operations defined in [11].

This work was supported by project 110287780575 through the agreement 785-2019 between the *Agencia Nacional de Hidrocarburos*, the *Ministerio de Ciencia, Tecnología e Innovación*, and *Fondo Nacional de Financiamiento para la Ciencia, la Tecnología y la Innovacion Francisco Jose de Caldas.*
T. Gelvez-Barrera is supported by Labex Celya.

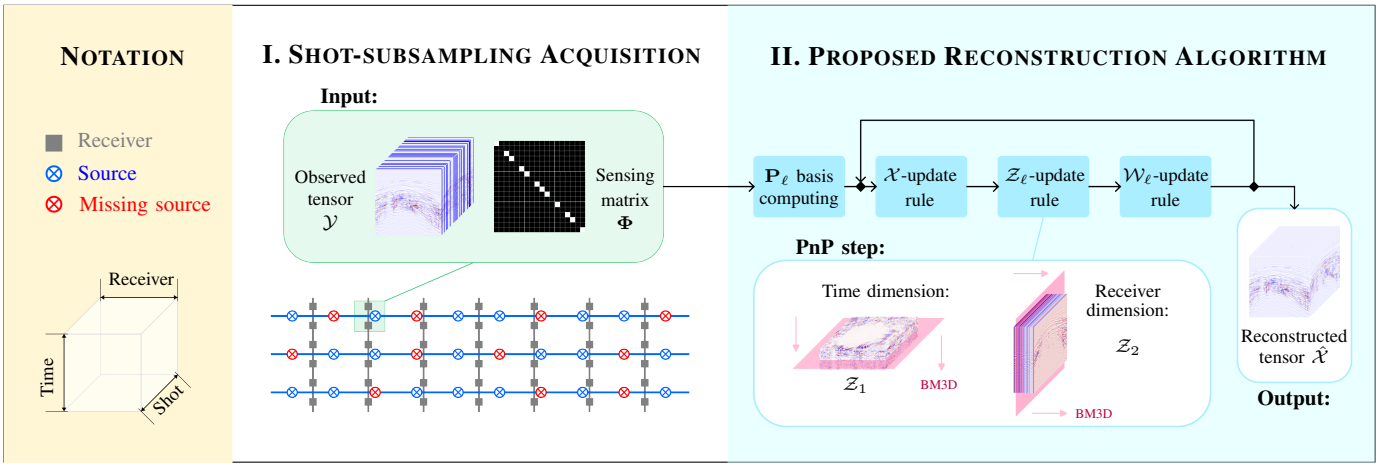

Fig. 1: Proposed method overview. Section I) represents the orthogonal seismic geometry with undetonated sources (shown in red). The input of the algorithm is the sensing matrix encoding the position of the missing shots. Section II) outlines the proposed reconstruction algorithm process. There, the PnP step is solved in two different tensor dimensions.

Figure 1 illustrates the proposed method, divided in the two following sections, the sub-sampling acquisition and the reconstruction algorithm.

A. Seismic Shot Sub-sampling Observation Model

Mathematically, let $\mathcal{X} \in \mathbb{R}^{I_1 \times I_2 \times I_3}$ define a 3D tensor that represents the seismic datacube of a cross-spread with I_2 receivers and I_3 sources, recorded in I_1 time samples.

The seismic acquisition observation model with sub-sampled shots, representing the phenomena when a certain number of sources are not detonated, can be mathematically formulated with the following tensor forward linear model

$$\mathcal{Y} = \mathcal{X} \times_3 \mathbf{\Phi}, \tag{1}$$

where $\mathcal{Y} \in \mathbb{R}^{I_1 \times I_2 \times I_3}$ denotes a 3D captured datacube with missing shots and $\mathbf{\Phi} \in \{0,1\}^{I_3 \times I_3}$ denotes the shot sub-sampling matrix. $\mathbf{\Phi}$ is a binary diagonal matrix encoding the detonated and undetonated shots with one and zero, respectively, where the zeros produce the missing shots in $\mathcal{Y}$. Figure 1 highlights as the input, an observed tensor with missing shots, as well as their corresponding sensing matrix.

B. Seismic Shot Recovery Problem Formulation

The seismic shot recovery is an ill-posed challenging inverse problem aiming to reconstruct the seismic datacube $\mathcal{X}$ from the captured datacube $\mathcal{Y}$ and the sub-sampling matrix $\mathbf{\Phi}$. To mitigate the ill condition, this work takes advantage of the self-similarities exhibited by the seismic features (i.e., hyperbolic and linear events), considering the high non-local redundancies in the structure of the underlying subsurface rocks, where the same seismic pattern can be found at different locations. The optimization problem for shot reconstruction is proposed as

$$\underset{\mathcal{X} \in \mathbb{R}^{I_1 \times I_2 \times I_3}}{\text{minimize}} \quad \frac{1}{2}\|\mathcal{Y} - \mathcal{X} \times_3 \mathbf{\Phi}\|_2^2 + \mu \|\mathcal{X}\|_{NL}, \tag{2}$$

where the first term corresponds to an ℓ_2-norm minimizing the distance between the observed and estimated incomplete datacube, ensuring the condition given in (1), and the second term corresponds to the non-local-norm regularizer defined in [12] promoting the NSS prior.

This work aims to promote the NSS over the different seismic datacube dimensions. A tensor factorization will be used to separate the regularizer in each independent dimension of the seismic datacube.

If $\mathcal{X} \in \mathbb{R}^{I_1 \times I_2 \times I_3}$ defines an arbitrary third-order tensor, then the $\ell^{th} \in \{1,2,3\}$ dimension of the tensor can be factorized with the m-mode product as

$$\mathcal{X} = \mathcal{Z}_\ell \times_\ell \mathbf{P}_\ell, \tag{3}$$

where $\mathbf{P}_\ell \in \mathbb{R}^{I_\ell \times r_\ell}$ defines a basis matrix and $\mathcal{Z}_\ell \in \mathbb{R}^{\tilde{I}_1 \times \tilde{I}_2 \times \tilde{I}_3}$ defines a coordinate tensor, with $\tilde{I}_\kappa = r_\ell$ when $\kappa = \ell$, and $\tilde{I}_\kappa = I_\kappa$ otherwise. Depending on the selection of the basis matrix $\mathbf{P}_\ell$, the tensor $\mathcal{Z}_\ell$ will exhibit certain properties. For instance, when $\mathbf{P}_\ell$ is computed with the r_ℓ most significant principal components of the matrix $\mathbf{X}_{[\ell]}$, the tensor $\mathcal{Z}_\ell$ preserves the spatial structures in the slices of the ℓ^{th} dimension.

Considering the factorization introduced in (3), the non-local-norm can be separated in two terms, for the temporal and receiver dimensions, as shown in Fig. 1, as

$$\mu\|\mathcal{X}\|_{NL} = \mu_1\|\mathcal{Z}_1 \times_1 \mathbf{P}_1\|_{NL} + \mu_2\|\mathcal{Z}_2 \times_2 \mathbf{P}_2\|_{NL}, \tag{4}$$

with the separation of the regularizer parameter $\mu = \mu_1 + \mu_2$. The formulation in (4) does not include the third dimension, i.e., the source dimension, because the seismic datacube is sub-sampled in this dimension, leading to an ill-conditioning problem in the factorization.

Notice that the non-local-norm in (4) is applied directly to the $\mathcal{Z}_\ell \times_\ell \mathbf{P}_\ell$ tensors, which is equivalent to compute the norm into $\mathcal{X}$. Nevertheless, it can be assumed that the NSS prior of $\mathcal{X}$ is preserved on the ℓ^{th} dimension slices of the coordinate tensors $\mathcal{Z}_\ell$, with a proper selection of $\mathbf{P}_\ell$. Therefore, the non-local-norm can be approximated as follows

$$\mu\|\mathcal{X}\|_{NL} \approx \mu_1\|\mathcal{Z}_1\|_{NL} + \mu_2\|\mathcal{Z}_2\|_{NL}. \tag{5}$$

Introducing the norm definition in (5), in the optimization problem (2), the proposed seismic shot reconstruction results in the following optimization problem with separated variables

$$\begin{aligned} \underset{\mathcal{X},\mathcal{Z}_\ell}{\text{minimize}} \quad & \frac{1}{2}\|\mathcal{Y}-\mathcal{X}\times_3\mathbf{\Phi}\|_2^2+\mu_1\|\mathcal{Z}_1\|_{NL}+\mu_2\|\mathcal{Z}_2\|_{NL} \\ \text{subject to} \quad & \mathcal{X}=\mathcal{Z}_1\times_1\mathbf{P}_1, \quad \mathcal{X}=\mathcal{Z}_2\times_2\mathbf{P}_2. \end{aligned} \tag{6}$$

C. Seismic Shot Recovery Numerical Algorithm

The proposed numerical algorithm follows the Alternating Direction Method of Multipliers (ADMM) framework to find the solution of the optimization problem formulated in (6), considering that the cost function is composed of a sum of independent terms with respect to each optimization variable.

The augmented Lagrangian of the problem is defined as

$$\begin{aligned} \mathcal{L}_\rho(\mathcal{X},\mathcal{Z}_\ell,\mathcal{W}_\ell) &= \frac{1}{2}\|\mathcal{Y}-\mathcal{X}\times_3\mathbf{\Phi}\|_2^2 \\ &+\mu_1\|\mathcal{Z}_1\|_{NL}+\frac{\rho}{2}\|\mathcal{X}-\mathcal{Z}_1\times_1\mathbf{P}_1+\mathcal{W}_1\|_2^2 \\ &+\mu_2\|\mathcal{Z}_2\|_{NL}+\frac{\rho}{2}\|\mathcal{X}-\mathcal{Z}_2\times_2\mathbf{P}_2+\mathcal{W}_2\|_2^2, \end{aligned} \tag{7}$$

where $\mathcal{W}_\ell \in \mathbb{R}^{I_1\times I_2\times I_3}$ are the dual variables for each constraint of the problem, and $\rho>0$ is the dual parameter that weights the importance of the constraint in the cost function.

The ADMM iteratively minimizes the augmented Lagrangian function in (7), updating each variable as follows

$$\mathcal{X}^{t+1} \in \arg\min_{\mathcal{X}} \ \mathcal{L}_\rho(\mathcal{X},\mathcal{Z}_\ell^t,\mathcal{W}_\ell^t) \tag{8}$$

$$\mathcal{Z}_\ell^{t+1} \in \arg\min_{\mathcal{Z}_\ell} \ \mathcal{L}_\rho(\mathcal{X}^{t+1},\mathcal{Z}_\ell,\mathcal{W}_\ell^t) \tag{9}$$

$$\mathcal{W}_\ell^{t+1}=\mathcal{X}^{t+1}-\mathcal{Z}_\ell^{t+1}+\mathcal{W}_\ell^t, \tag{10}$$

for indexes $\ell\in\{1,2\}$.

The update details defined in (8)-(10) are summarized in Algorithm 1. There, line 1 computes the basis matrices $\mathbf{P}_\ell$ from the r_ℓ principal components of the unfolding matrix of $\mathcal{Y}$ on the ℓ^{th} dimension. Lines 3-4 initialize the $\mathcal{Z}_\ell$ variables from the tensor $\mathcal{Y}$ and the dual variables $\mathcal{W}_\ell$ as null tensors. Line 7 updates $\mathcal{X}$ following the optimization problem in (8), involving a differentiable function composed of the summation of three tensors ℓ_2 norms. Hence, (8) is solved using a closed solution by finding the zeros of the derivative of the cost function. Lastly, line 8 updates the auxiliary variables $\mathcal{Z}_\ell$ by solving an optimization problem with the form

$$\underset{\mathcal{Z}_\ell}{\text{minimize}} \quad \frac{\rho}{2}\|\mathcal{X}^{t+1}-\mathcal{Z}_\ell\times_\ell\mathbf{P}_\ell+\mathcal{W}_\ell^t\|_2^2+\mu_\ell\|\mathcal{Z}_\ell\|_{NL}, \tag{11}$$

reformulated as a proximal operator optimization given by

$$\underset{\mathcal{Z}_\ell}{\text{minimize}} \quad \frac{1}{2\sigma_\ell^2}\|\mathcal{Z}_\ell-(\mathcal{X}^{t+1}+\mathcal{W}_\ell^t)\times_\ell\mathbf{P}_\ell^\top\|_2^2+\|\mathcal{Z}_\ell\|_{NL}, \tag{12}$$

where $\sigma_\ell=\sqrt{\mu_\ell/\rho}$ defines the parameter related to the proximal operator. Equation (12) connotes that $\mathcal{Z}_\ell$ is a noisy version of $(\mathcal{X}^{t+1}+\mathcal{W}_\ell^t)\times_\ell\mathbf{P}_\ell^\top$, so that, the problem can be solved by the PnP methodology using a greedy denoising algorithm. In particular, this work adopted the channel-wise BM3D denoiser [13] considering the patch-based nature of the algorithm, where the block-matching step leads to promoting the NSS prior. Therefore, the solution of (12) can be approximated by

$$\mathbf{Z}_\ell=\text{BM3D}_\ell\left((\mathcal{X}^{t+1}+\mathcal{W}_\ell^t)\times_\ell\mathbf{P}_\ell^\top,\sigma_\ell\right), \tag{13}$$

with $\text{BM3D}_\ell(\cdot)$ defining the BM3D applied through the time or receiver slices for $\ell=1$ and $\ell=2$, respectively.

Algorithm 1: Seismic shot reconstruction algorithm

Input: Acquisition data: $\mathcal{Y},\mathbf{\Phi}$.
Algorithm parameters: $\rho,\mu_\ell,r_\ell,n_{iter}$.
Output: Reconstructed cube $\mathcal{X}^{n_{iter}}$

```
/* PCA as the selected transformation basis */
1  P_ℓ ← PCA(Y_[ℓ], r_ℓ)
2  t ← 0
3  Z_ℓ^t ← Y ×_ℓ P_ℓ^⊤
4  W_ℓ^t ← 0
5  while t < n_iter do
6      S^t ← Z_1^t ×_1 P_1 + Z_2^t ×_2 P_2 − W_1 − W_2
7      X^{t+1} ← (Y + ρS^t) ×_3 (Φ + 2ρI)^{-1}
8      Z_ℓ^{t+1} ← BM3D_ℓ((X^{t+1} + W_ℓ^t) ×_ℓ P_ℓ^⊤, σ_ℓ)
9      W_ℓ^{t+1} ← X^{t+1} − Z_ℓ^{t+1} + W_ℓ^t
10     t ← t + 1
```

III. Simulations and Results

This section measures the performance of the proposed algorithm and the comparison of the quality results against various data completion algorithms in the literature.

A. Experimental design

The experiments employ the "SEAM Phase II–Land Seismic Challenges, Foothills model" dataset [14], a synthetic-realistic acquisition, including sharp topography, soft alluvial fill at the surface, and complex structures at depth features. A datacube with 61 shots was resized to 128×128 time and receiver samples, given that some comparison methods require dyadic dimensions. In the simulations, 25% of the shots were removed from the seismic datacube in a randomized scheme following the formulation in (1), and then reconstructed by each method.

This work builds a comparative benchmark adapting state-of-the-art reconstruction methods, given that the seismic shot reconstruction problem has not been widely addressed. The algorithms used in the comparison benchmarking are: the consensus equilibrium (CE) [6], using multiple regularizers for the shot reconstruction problem; the multichannel singular spectrum analysis (MSSA) [15], using rank-reduction to reconstruct 1D columns in the seismic datacube; an interpolation neural network using a ResNET proposed in [16], where the model was trained taking advantage of the similarities between the shots and receiver slices; and a traditional optimization promoting a sparsity prior solved with an ADMM algorithm.

The reconstruction quality is measured in terms of: the mean-squared error (MSE), quantifying the value-to-value

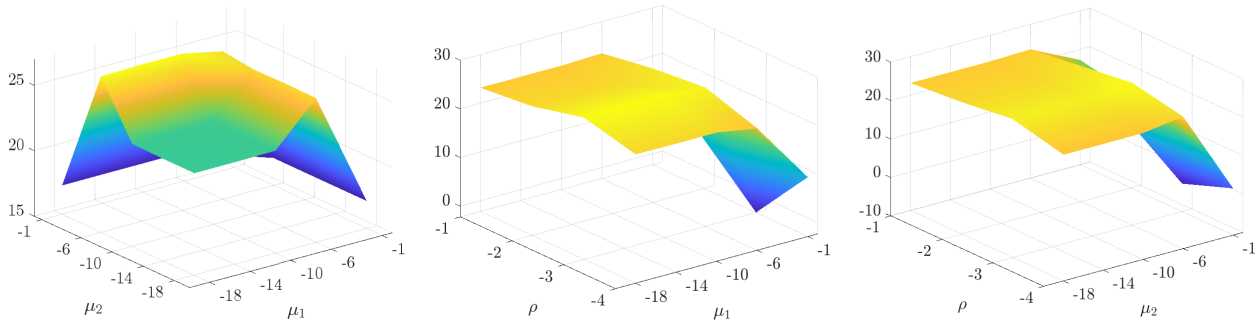

Fig. 2: Surface plot of the reconstruction PSNR for different values of μ_1, μ_2, and ρ. The μ_ℓ values are in the $[10^{-18}, 10^{-1}]$ logarithmic range, and ρ in the $[10^{-4}, 1]$ logarithmic range. The x and y axis represent the order for the μ_1, μ_2, and ρ parameters, and the z axis represents the obtained PSNR. A smooth variation across the evaluated parameters can be observed, achieving the highest values for $\rho = 0.001$ and μ_ℓ in the 10^{-6} order.

difference; the peak signal-to-noise ratio (PSNR) and the signal-to-noise ratio (SNR), measuring the power of the reconstruction error with respect to the desired signal; and the structural similarity index (SSIM), measuring the similarity in the inner structures and events of the shots. Additionally, the computing time was recorded in each simulation.

B. Algorithm setup

The regularization parameters selection is a critical issue in the ADMM-PnP approach. Therefore, the proposed algorithm parameters were selected through a cross-validation strategy to find the best configuration. The non-local regularizer parameters μ_ℓ were varied in a logarithmic scale in the $[10^{-18}, 10^{-1}]$ range, and the dual parameter in the $[10^{-4}, 1]$ range.

Figure 2 depicts a surface showing the results of the cross-validation process. There, a smooth behavior can be seen around an optimal pair of parameters, where the highest quality reconstruction is achieved when both μ_ℓ parameters are in the order 10^{-6}. Furthermore, notice that the proposed algorithm is sensitive to the dual parameter, marking a significant quality difference for reconstructions using $\rho = 10^{-3}$.

Besides, the number of principal components used in the matrix basis $\mathbf{P}_\ell$ was tuned to $r_\ell = 75$ after cross-validation of 25 r_ℓ values uniformly distributed in the range $[5, 100]$. Although the PnP strategy does not guarantee algorithm convergence, it was determined experimentally that for a number of 200 iterations, the algorithm reached a stable solution.

The CE method's parameters were tuned using a cross-validation procedure following the referenced metrics in the author's paper. In the MSSA algorithm, the rank parameter was varied in the range $[5, 80]$ with a 5-unit step and the selected frequencies in the $[0, 80]$ range. For the ResNET, the network architecture and optimizer were selected as in [16]. Lastly, the sparsity regularization parameter in the ADMM method was varied in a logarithmic scale in the $[10^{-5}, 10^{-0.5}]$ range, and the dual parameter was varied uniformly in the range $[0.5, 1.5]$, taking 10 values from the range in each case.

TABLE I: Quantitative seismic shot reconstruction results. The MSE is scaled in the 10^{-3} order. The PSNR and SNR are measured in decibels [dB], and the computation time is measured in seconds [s].

	Proposed	**CE** [6]	**ResNET** [16]	**MSSA** [15]	**ADMM**
MSE$^{\downarrow}$	**1.54**	2.29	21.57	2.20	2.87
PSNR$^{\uparrow}$	**28.12**	26.40	16.66	26.57	25.42
SNR$^{\uparrow}$	**22.18**	20.45	10.71	20.62	19.47
SSIM$^{\uparrow}$	**0.81**	0.74	0.37	0.65	0.53
Time	**808**	3305	6262	5362	2752

C. Shot reconstruction results

Table I summarizes the results of the simulations carried out to measure the performance of the proposed algorithm against the comparative benchmark. The proposed algorithm outperforms the literature methods for all evaluated metrics, obtaining a gain of up to 1.55 [dB] of PSNR and 0.06 of SSIM. The gain in the SSIM can be interpreted as an improved ability of the algorithm to reconstruct the internal structures exhibited in the missing shots, which is essential for good-quality surface image generation and analysis. Likewise, Table I compares the execution time to measure computational complexity, where the developed algorithm presents a significant reduction in computing time.

Figure 3 visually compares the structures in the reconstructed shots. The first row shows an amplitude map of a reconstructed shot by each method; the second row shows two zoom sections showing important differences between the reconstructions; and the third row shows the absolute error map between the reconstructed and ground-truth shot.

The shots reconstructed by the proposed algorithm exhibit a better definition of the seismic events, presenting a lower error in the peaks of the events compared to the other methods. The cyan section highlights two important features. In the right part, a set of events are well reconstructed with the proposed method, while the same events are estimated with very reduced amplitudes or lost completely as in the ResNET and ADMM cases; on the other hand, the left part shows noise, well reduced by the proposed method, while intensified by the others. The red section shows well-reconstructed events using the proposed method, while the comparison methods have a loss of amplitudes. The absolute error maps report the amount

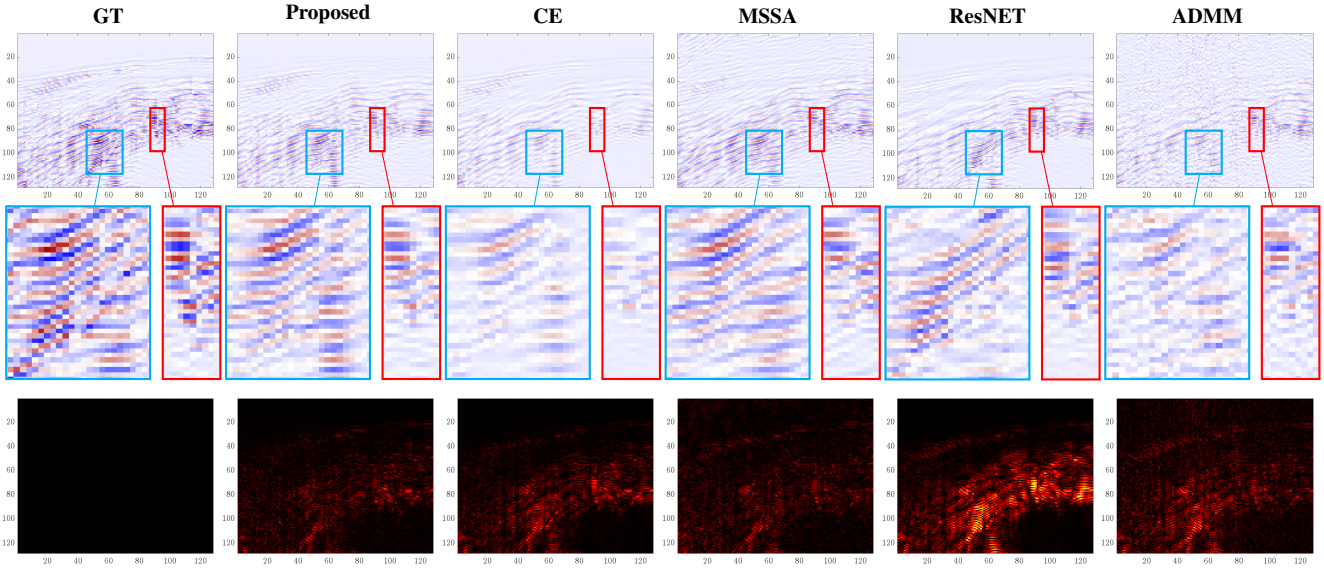

Fig. 3: Seismic shot visual reconstructions. Each column presents the results using a different method. The first row shows one reconstructed shot in the amplitude domain. The second-row zooms in and highlights the reconstruction differences in two shot sections. The third row reports the normalized absolute difference between the reconstruction and the ground truth.

of missing information for all the methods, with the highest errors located in the highlighted sections. Notice that the ResNET error map presents the highest values, showing that its performance is affected by poor amplitudes reconstruction.

IV. Conclusions

This work proposed a seismic shot reconstruction algorithm that takes advantage of the non-local self-similarity property present in the time and receiver dimension of the seismic datacube in the cross-spread domain. Specifically, a PnP methodology is flexibly introduced in an ADMM algorithm using a low-rank tensor factorization to apply the non-local prior through two different dimensions. Simulations show that the proposed algorithm achieves better reconstructions than the methods in the comparative benchmark in an experiment with 25% of sub-sampled shots. Experimentally, the developed algorithm has a faster execution time compared with the specialized seismic interpolation methods; this is, the use of the PCA tensor factorization, unlike the sparse transformation in CE algorithm [6], helps to reduce computational complexity and achieve reconstructions with lower loss of seismic events information. Finally, the regularization parameter setup of the proposed algorithm was analyzed through a cross-validation methodology, where slight variations in the dual parameter were found to produce a significant difference in the quality of the reconstructed shots.

References

[1] C. L. Liner, *Elements of 3D seismology*. Society of Exploration Geophysicists, 2016.

[2] G. Vermeer, "Understanding the fundamentals of 3d seismic survey design," *first break*, vol. 19, no. 3, 2001.

[3] O. Villarreal, K. León-López, D. Espinosa, W. Agudelo, and H. Arguello, "Seismic source reconstruction in an orthogonal geometry based on local and non-local information in the time slice domain," *Journal of Applied Geophysics*, vol. 170, p. 103846, 2019.

[4] Y. Chen, X. Chen, Y. Wang, and S. Zu, "The interpolation of sparse geophysical data," *Surv. in Geophysics*, vol. 40, no. 1, pp. 73–105, 2019.

[5] O. P. Villarreal, K. León, D. Espinosa, W. Agudelo, and H. Arguello, "Compressive sensing seismic acquisition by using regular sampling in an orthogonal grid," in *7th Int. Workshop on Computational Advances in Multi-Sensor Adaptive Processing (CAMSAP)*, pp. 1–5, IEEE, 2017.

[6] P. Goyes-Peñafiel, E. Vargas, C. V. Correa, W. Agudelo, B. Wohlberg, and H. Arguello, "A consensus equilibrium approach for 3d land seismic shots recovery," *IEEE Geoscience and Remote Sensing Lett.*, vol. 19, pp. 1–5, 2021.

[7] S. Rivera, I. Ortiz, T. Gelvez-Barrera, L. Galvis, and H. Arguello, "Seismic source recovery algorithm via internal learning in the cross-spread domain," in *Fourth HGS/EAGE Conference on Latin America*, vol. 2022, pp. 1–5, EAGE Publications BV, 2022.

[8] R. Anvari, M. Mohammadi, J. Mafakheri, A. Roshandel Kahoo, M. Soleimani Monfared, S. Rashidi, and A. H. Mohammed, "Denoising of multidimensional seismic data in the physical domain by a new non-local self similarity method," *Earth Science Informatics*, pp. 1–20, 2022.

[9] T. Gelvez and H. Arguello, "Nonlocal low-rank abundance prior for compressive spectral image fusion," *IEEE Trans. on Geoscience and Remote Sensing*, vol. 59, no. 1, pp. 415–425, 2020.

[10] T. Gelvez-Barrera, H. Arguello, and A. Foi, "Joint nonlocal, spectral, and similarity low-rank priors for hyperspectral–multispectral image fusion," *IEEE Trans. on Geoscience and Remote Sensing*, vol. 60, pp. 1–12, 2022.

[11] T. G. Kolda and B. W. Bader, "Tensor decompositions and applications," *SIAM review*, vol. 51, no. 3, pp. 455–500, 2009.

[12] W. He, Q. Yao, C. Li, N. Yokoya, Q. Zhao, H. Zhang, and L. Zhang, "Non-local meets global: An iterative paradigm for hyperspectral image restoration," *IEEE Trans. on Pattern Analysis and Machine Intelligence*, vol. 44, no. 4, pp. 2089–2107, 2020.

[13] K. Dabov, A. Foi, V. Katkovnik, and K. Egiazarian, "Image denoising by sparse 3-d transform-domain collaborative filtering," *IEEE Trans. on image processing*, vol. 16, no. 8, pp. 2080–2095, 2007.

[14] C. Regone, J. Stefani, P. Wang, C. Gerea, G. Gonzalez, and M. Oristaglio, "Geologic model building in seam phase ii—land seismic challenges," *The Leading Edge*, vol. 36, no. 9, pp. 738–749, 2017.

[15] Y. Chen, W. Huang, D. Zhang, and W. Chen, "An open-source matlab code package for improved rank-reduction 3d seismic data denoising and reconstruction," *Computers & Geosciences*, vol. 95, pp. 59–66, 2016.

[16] B. Wang, N. Zhang, W. Lu, J. Geng, and X. Huang, "Intelligent missing shots' reconstruction using the spatial reciprocity of green's function based on deep learning," *IEEE Trans. on Geoscience and Remote Sensing*, vol. 58, no. 3, pp. 1587–1597, 2019.